# Cell Entry of One-Dimensional Nanomaterials Occurs by Tip Recognition and Rotation

## Supplemental Information

Xinghua Shi[1,4], Annette von dem Bussche[2], Robert H. Hurt[1,3], Agnes B. Kane[2,3], Huajian Gao[1,3]

[1]School of Engineering, Brown University, Providence, RI 02912, USA
[2]Department of Pathology and Laboratory Medicine, Brown University, Providence, RI 02912, USA
[3]Institute for Molecular and Nanoscale Innovation, Brown University, Providence, RI, 02912, USA
[4]Present address: State Key Laboratory of Nonlinear Mechanics, Institute of Mechanics, Chinese Academy of Sciences, Beijing 100190, China.

### *Cell experiments*

Additional experiments were conducted to assess whether the uptake of cylindrical nanomaterials can be attributed to energy dependent endocytosis. We exposed AML12 cells to 80 ppm MWCNTs for 2 hours at 4°C and as control at 37°C. The numbers of tubes taken up by the cells was determined by confocal microscopy and image analysis (see Methods) using crossed polarizing light filters, which is an imaging mode that allows identification of the tubes through birefringence (Supp. Fig. 1a). Before counting, the cells were exposed to FITC-conjugated anti-tubulin antibodies and stained with DAPI to visualize the cytoskeleton and nucleus in the confocal images in order to distinguish internalized from extracellular nanotubes. A second test for energy-dependent endocytosis was carried out by preincubation of AML12 cells with metabolic inhibitors (0.02 % sodium azide, 1.875 mM sodium fluoride and 0.25 ug/ml Antimycin A) for 30 min followed by exposure to 80 ppm MWCNTs for 2 hours. After staining with FITC conjugated anti-tubulin antibodies and DAPI the uptake of MWCNTs was again determined by confocal microscopy with using polarized light filters (Supp. Fig. 1b). Uptake is suppressed both by temperature reduction and by metabolic inhibitors, consistent with a mechanism of energy-dependent endocytosis.

Cell viability in both experiments was confirmed using the Pico Green Assay (Invitrogen) to quantify DNA content (Supp. Fig. 1). Supp. Fig. 2 shows the tubulin and nuclear fluorescence

for intracellular localization of MWCNTs using confocal microscopy, and results of an ATP assay that confirms the activity of the metabolic inhibitors for murine liver cells.

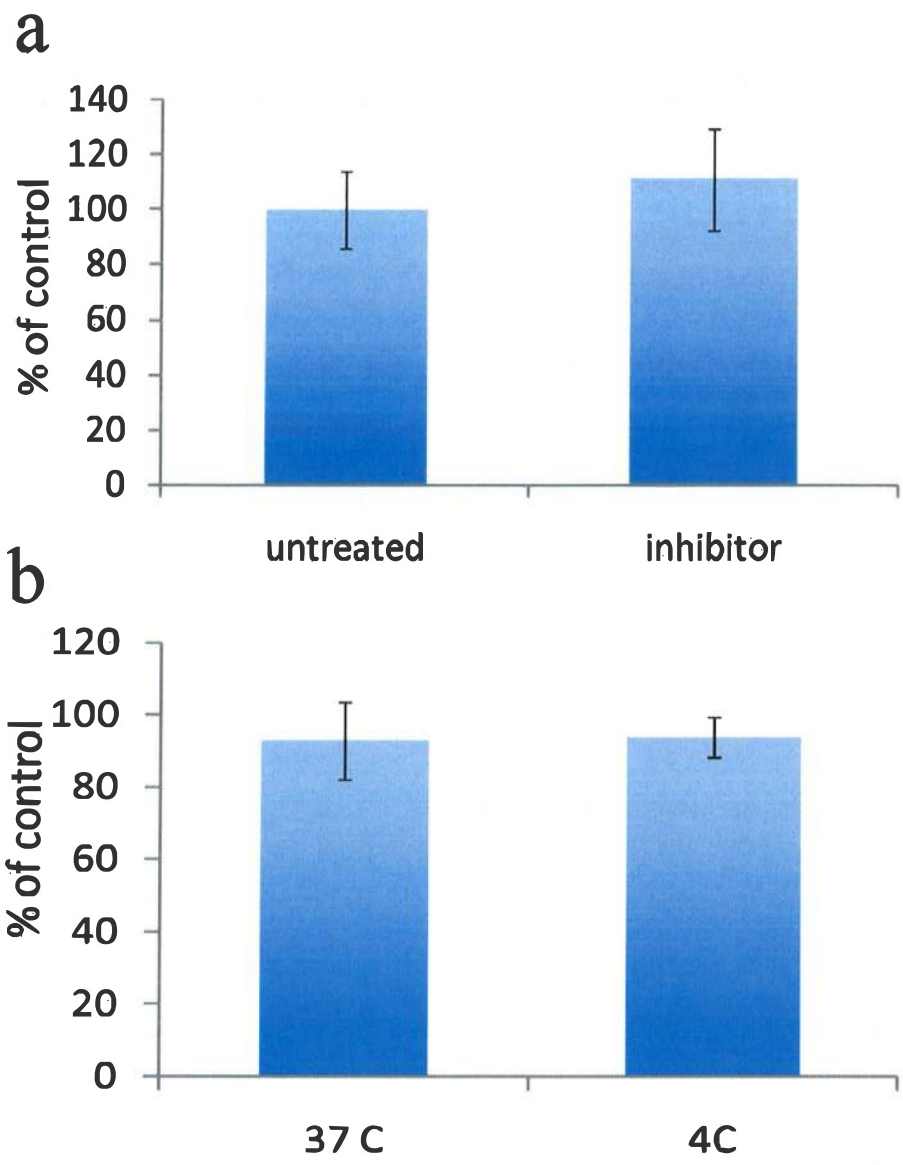


**Supplementary Figure 1. Determination of cell viability using the Pico Green assay.** **a,** After treatment with inhibitors. **b,** After temperature reduction to 4°C.

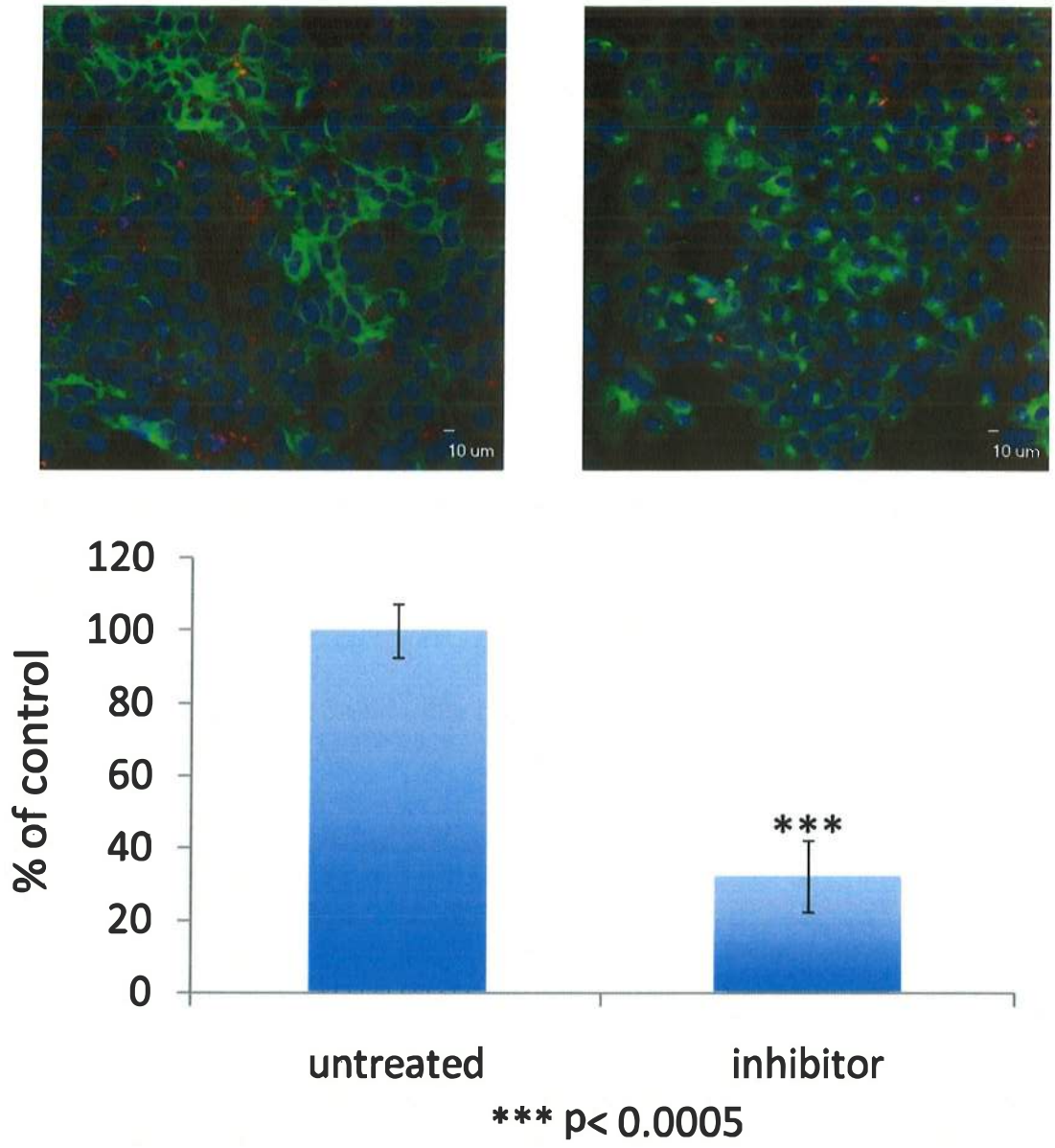


**Supplementary Figure 2.** Top: Confocal image after exposure of murine liver cells to 80 ppm MWCNTs for 2hrs at 37°C or at 4°C. Blue fluorescence (DAPI nuclear stain), green fluorescence (anti-tubulin antibody), and red (polarized light confocal microscopy). Red spots/lines show MWCNTs co-localized with the cytoplasm or nucleus in the image plane, and are much more abundant at 37°C than at 4°C. Bottom: Cells exposed to metabolic inhibitors for 2.5 hours were assessed for ATP content using luminescence based assay, confirming the effectiveness of the metabolic inhibitors.

### *Additional Modes of Nanomaterial-Membrane Interaction*

In addition to the dominant tip-entry mode seen for cylindrical, one-dimensional nanomaterials, the electron microscopy reveals other, less common modes of interaction. Supp. Fig. 3 shows

MWCNTs lying parallel and apparently adhered to the cell membrane, but with no evidence of active wrapping or uptake (Supp. Fig. 3a). Much less common is the observation of active membrane interaction with these side-wall adhered tubes, and Supp. Fig. 3b shows this behavior as a counter example to the dominant tip-entry behavior.


**Supplementary Figure 3. Examples of non-tip-based interactions with mouse liver cells.** **a,** Common observation of nanotubes lying flat on outer cell membrane, but without apparent active uptake. Side-wall contact appears to cause membrane attachment, but not to trigger endocytosis. **b,** Uncommon structure shown as a counter example, of partial wrapping by the cell membrane of a side-wall-attached MWCNT.

***Simulations***

In our coarse-grained molecular dynamics (CGMD) simulations, the bead-bead interactions are described by the following potentials:

$$U_{WCA}(r) = 4\varepsilon\left[\left(\frac{b}{r}\right)^{12} - \left(\frac{b}{r}\right)^{6} + \frac{1}{4}\right] \quad \left(0 < r < r_{\text{cut}} = 2^{1/6}b\right),$$

$$U_{COS}(r) = \begin{cases} -\varepsilon + U_{WCA}(r) & \left(r < r_{cut} = 2^{1/6}\sigma\right) \\ -\varepsilon\cos^2\dfrac{\pi(r - r_{cut})}{2w} & \left(r_{cut} \le r \le r_{cut} + w\right) \end{cases},$$

$$U_{FENE}(r) = -\frac{1}{2}k_{FENE}r_{\infty}^2 \ln\left(1 - \frac{r^2}{r_{\infty}^2}\right) \quad (0 < r < r_{\infty}).$$

(Eq. S1)

In the following, $\varepsilon$ and $\sigma$ are used as the units of energy and length. To construct the bilayer with an appropriate thickness, the bead diameter, $\sigma$, is set at 1 nm. The parameter $\varepsilon$ can be

deduced from temperature, which is set at $k_B T = 1.1\varepsilon$. For lipids, the nearest neighbor beads are connected by FENE bonds with $k_{FENE} = 30\varepsilon$ and $r_\infty = 1.5\sigma$. The head bead is also connected with the second tail bead by a harmonic potential with rest length $r_0 = 4\sigma$ and force constant $k_{bend} = 10\varepsilon$. The non-bonded interaction parameters are listed inSupplementary Table1.

**Supplementary Table 1: Parameters of non-bonded interactions**

| bead type | bead type | interaction | parameters |
|---|---|---|---|
| lipid/receptor head | lipid/receptor head | WCA | $b = 0.95\sigma$ |
| lipid/receptor head | lipid/receptor tail | WCA | $b = 0.95\sigma$ |
| lipid/receptor tail | lipid/receptor tail | COS | $b = \sigma, w = 1.6\sigma$ |
| lipid head | CNT | WCA | $b = 0.95\sigma$ |
| receptor head | CNT | COS | $b = \sigma, w = 1.6\sigma$ |
| lipid tail | CNT | WCA | $b = 0.95\sigma$ |
| receptor tail | CNT | WCA | $b = 0.95\sigma$ |

***Flux of receptors***

With the parameters fixed as shown above, the receptor diffusivity can be determined, which is important in the present work. We quantitatively calculate the mean square displacement (MSD) of receptors within the planar bilayer through $MSD = \left\langle |r(t) - r(0)|^2 \right\rangle$ , where $\langle\ \rangle$ denotes the averaging over all the receptors, $r$ is the position of receptor and $t$ the time. The receptor diffusivity $D$ is connected to $MSD$ through $D = \lim_{t\to\infty} \frac{MSD}{4t}$. Supp. Fig. 4 shows the relation between $MSD$ and time $t$ when the fraction of receptor $\phi = 0.1$. The resulting diffusivity $D$ is about $0.97\times10^6$ $nm^2s^{-1}$, two orders higher than reported experimental values ($1\times10^4$ $nm^2s^{-1}$) [S1, S2]. We attribute this to the relatively small size of receptor in our model, which is designed to accelerate the simulation. Meanwhile, the density of receptor is also selected high to achieve the same goal. With the receptor fraction selected as $\phi = 0.1$, the density is about $8\times10^4$ $\mu m^{-2}$ in our model, two orders higher than the experimental one ($5\times10^2$ $\mu m^{-2}$) [S3, S4].

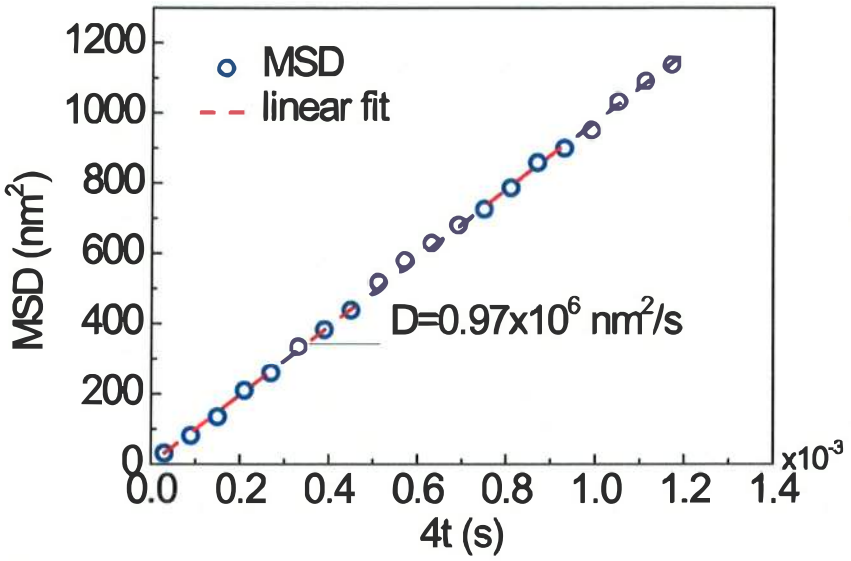


**Supplementary Figure 4. Mean square displacement (MSD) of receptors within the bilayer as a function of simulation time.** The fraction of receptors here is $\phi = 0.1$. The blue open circles are the calculated results and the red dash line is the fitting line.

The two factors, diffusivity and receptor density, greatly influence the flux of receptors entering the contact zone. Supp. Fig. 5a shows that receptor fluxes are much higher for high receptor density, but only at short times. For instance, the initial flux is about 20 $\mu s^{-1}$ when $\phi = 0.33$, and 3 $\mu s^{-1}$ when $\phi = 0.1$. As the fluxes decay exponentially in all three cases, they reach steady state and show only minor differences thereafter. This indicates that the receptor density has large influence on the flux primarily in the initial phase of the uptake process. We have also calculated the rates of receptor diffusion to the high and low angle sides of the tube. Supp. Fig. 5b shows that, at receptor density $\phi = 0.25$, the initial flux is much higher at the low angle side of the tube. However, it decays quickly and reaches a steady state similar to that on the high angle side of the tube. These results all consistently suggest that the receptor flux is limited by diffusion from the far field after a depletion zone is set up near the tube.

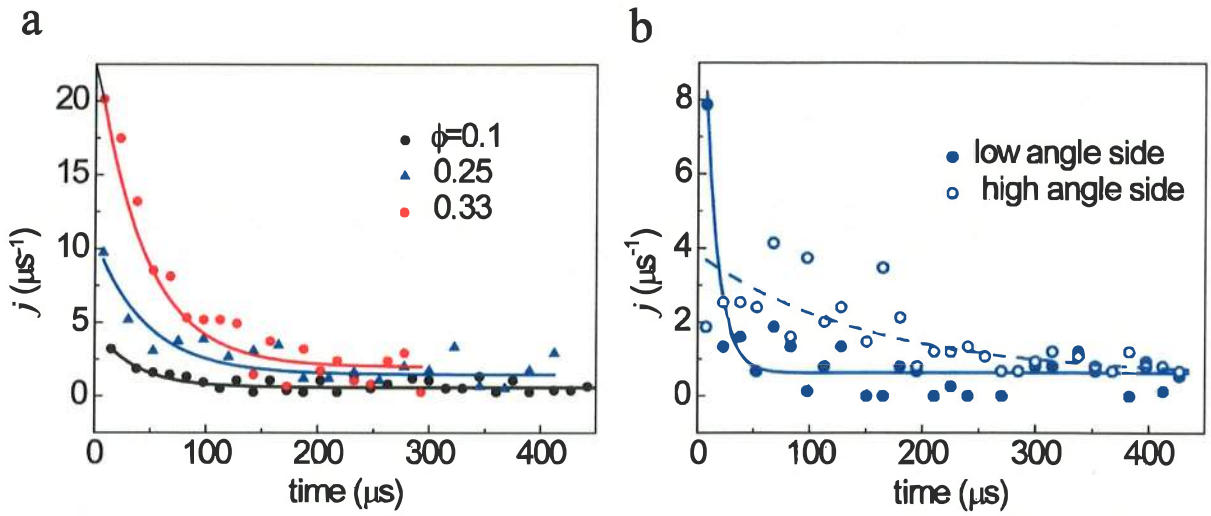


**Supplementary Figure 5. The evolution of receptor fluxes during cell uptake of a multi-walled carbon nanotube.** **a,** Receptor fluxes diffusing into the contact zone at different receptor densities $\phi = 0.1, 0.25, 0.33$. **b,** The receptor fluxes to the low angle side (solid) and high angle side (open) of nanotube at receptor density $\phi = 0.25$.

***Influence of CNT cap geometry***

Since membrane wrapping and uptake are initiated by receptor binding to CNT caps, it is important to explore whether the tip entry mechanism is sensitive to different cap geometries or tip structures. Our previous simulations (main text) were all for hemispherical caps, which is one of several common tip geometries. Supp. Fig. 6 compares the uptake mode for three alternative tip geometries: enlarged caps representing catalyst particles covered with graphenic carbon shells (6a); the complex tip geometry associated with a CNT bundle (6b) and open tips representing cut or oxidized CNTs (6c).

Supp. Fig. 6a shows a nanotube capped with an enlarged shell of diameter 30 nm interacting with a membrane patch with receptor fraction $\phi = 0.1$. In this case, the entry pathway is similar to that shown in Figure 3, with the nanotube rotating to 90° and undergoing tip-first entry. The uncapped (open) CNT does not rotate to a high angle, but rather sinks into the membrane with its axis parallel to the surface (Supp. Fig. 6c). This behavior was unexpected, but we believe the mechanism is apparent – the lack of carbon atoms at the tip prevents receptor adhesion necessary to initiate the tip wrapping and rotation. The receptors in the contact zone may only adhere to carbon atoms on the side wall, which preferentially pulls the nanotube parallel on the

membrane. Supp. Fig. 6b shows the behavior for a bundle of flat, but filled CNTs, which involves rotation to high angle similar to the base case of a single hemispherical cap. These simulations indicate that the tip shape has minor effect on the entry pathway as long as it is capped or filled. The pathway may change for uncapped, open tubes, which is an interesting prediction worthy of further study, and may provide a materials-based method for controlling cell entry.

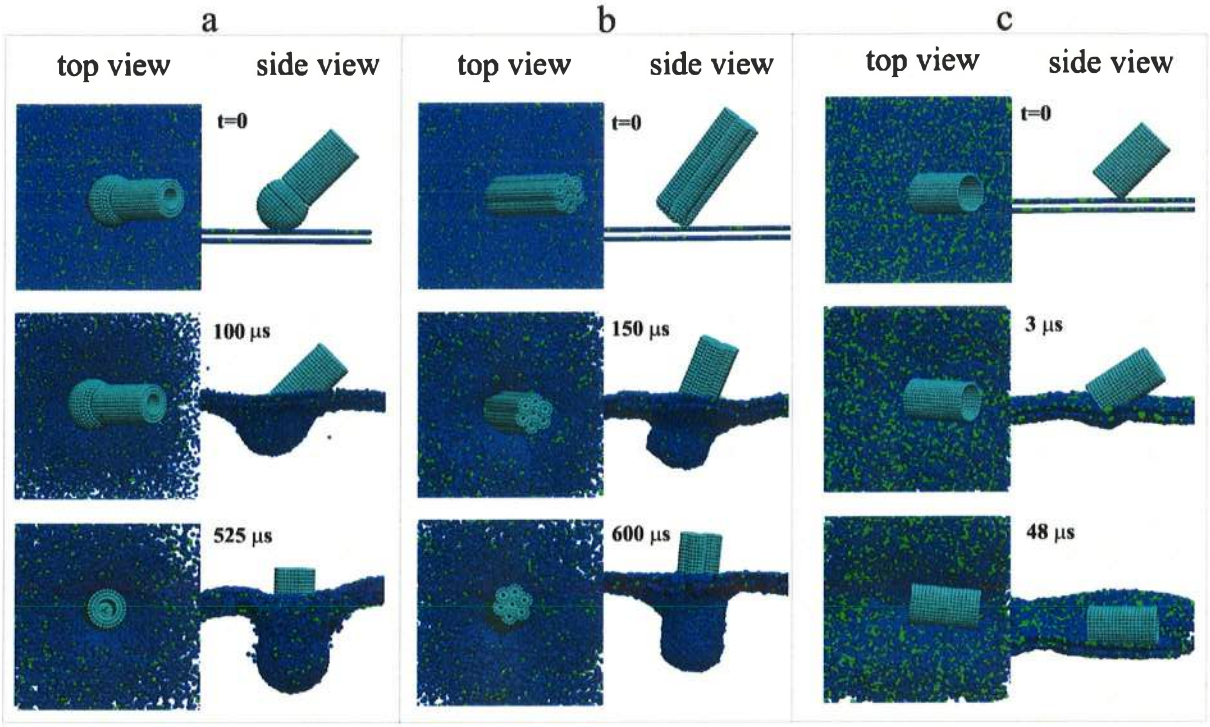


**Supplementary Figure 6. Time sequences of CGMD simulations showing nanotubes with different caps interacting with the cell membrane at an initial entry angle of** $\theta = 45^{\circ}$. **a,** Nanotube capped with an enlarged graphenic shell of diameter 30 nm. The fraction of receptorsis $\phi = 0.1$. **b,** Nanotube bundle interacting with the membrane at receptor fraction of $\phi = 0.1$. **c,** Uncapped, open nanotube interacting with the membrane at receptor fraction of $\phi = 0.25$

***Size effect***

In most of our simulations, we used a relatively small patch of bilayer of planar size 100 nm×100 nm and nanotubes of diameter 20 nm and length 46 nm. To investigate size effects, we conducted additional simulations with a larger membrane patch size of 200 nm×200 nm and a largercylindrical tube of diameter 40 nm and length 120 nm. It is observed that the long, thick

nanotube still rotates toward 90 degree, indicating a tip entry pathway (Supp. Fig. 7). It is important to know if the entry pathway is dependent on material diameter. It has been shown that sufficiently small nanoparticles may passively diffuse across through the membrane [S5] and that there exists a critical diameter on the order or 3-4 nm for a nanotube to change its pathway from wrapping to diffusion or piercing [S6]. The nanotubes used in our experiments have diameter in the range of 50-100 nm, and are expected to enter cell via wrapping. On the other hand, a bundle of very thin tubes are also expected to enter cell via wrapping, as shown in Supp. Fig. 6b.

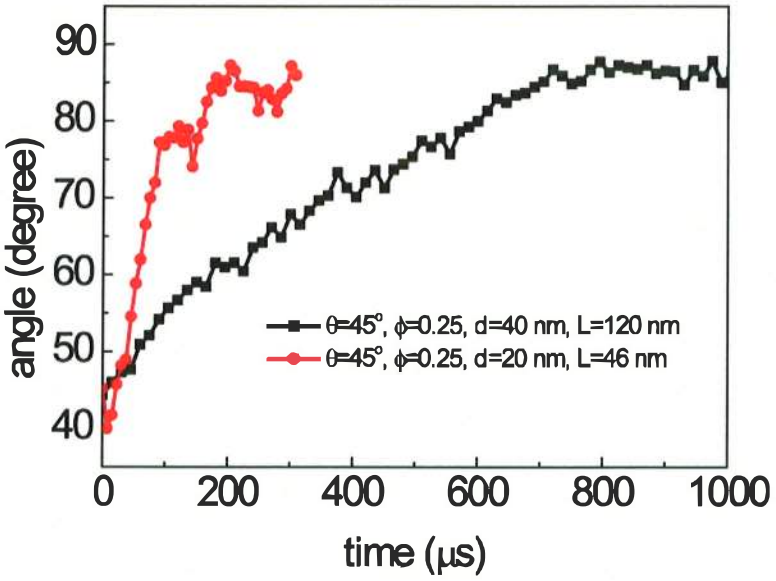


**Supplementary Figure 7. Evolution of the entry angle for nanotubes of different diameter.** Red curve: CNT diameter 20 nm and length 46 nm; Black curve: CNT diameter 40 nm and length 120 nm.

***Aspect ratio effect***

To investigate if the aspect ratio of a slender nanotube (or more generally a 1D nanomaterial) would affect its internalization mechanism, we performed the following two sets of simulations. In one set of the simulations, we constructed three nanotubes with different lengths 20 nm, 40 nm and 80 nm, but a fixed diameter of 20 nm. All three tubes had a hemispherical cap of diameter 20 nm. These tubes were allowed to interact with a 100 nm×100 nm membrane patch at an initial entry angle of 45 degree. In another set of simulations, we constructed two

nanotubes with different lengths 40 nm and 80 nm, but a fixed diameter of 40 nm. These tubes had a hemispherical cap of diameter 40 nm and were allowed to interact with a larger membrane patch of size 150 nm×150 nm. The receptor densities were set to be 0.1 in all simulations. Supp. Fig. 8 shows that the tubes with different aspect ratios all rotate to 90 degree, indicating that the tip-entry mechanism for the capped nanotubes is aspect ratio independent. We observed from the first set of simulations that the tube with higher aspect ratios needs longer time to rotate to 90 degree than that with lower aspect ratios (see Supp. Fig. 8). This is perfectly consistent with our expectation that longer tubes should encounter more viscous resistance during rotation. We also found that for the same aspect ratio, the rotating rate can also strongly depend on the size of the tube (e.g., compare the two curves associated with the aspect ratio (1:2) in Supp. Fig. 8), which is also consistent with our expectations.

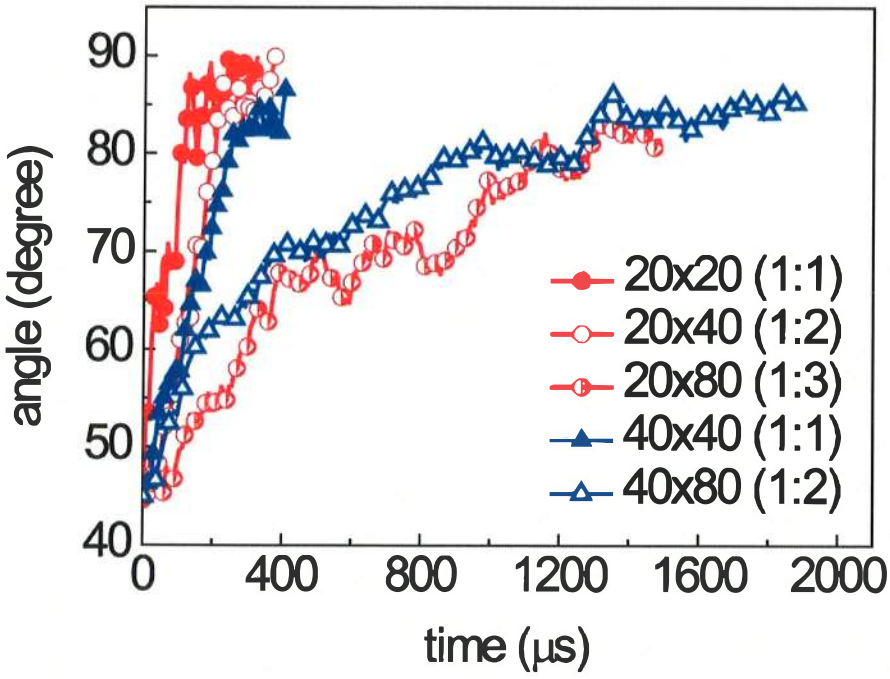


**Supplementary Figure 8. Evolution of the cell entry angle for nanotubes of different sizes and aspect ratios.** Red solid circle: diameter 20 nm and length 20 nm; red open circle: diameter 20 nm and length 40 nm; red half open circle: diameter 20 nm and length 80 nm; blue solid triangular: diameter 40 nm and length 40 nm; blue open triangular: diameter 40 nm and length 80 nm. The density of receptor in all simulations is set at 0.1.

***Initial entry angle effect***

To investigate the influence of the initial entry angle, we repeated the simulations for a relatively large initial angle of $\theta_0$=85° and a much smaller initial angle of $\theta_0$=15°. For $\theta_0$=85°, Supp. Fig. 9a shows that at $t$=120 μs, the entry angle is similar to the case of $\theta_0$=45° when $t$=120 μs (Fig. 3a), implying that the tube rotates faster at smaller initial entry angles. After $t$=120 μs, the entry angle continues to rotate toward 90° (Supp. Fig. 9a). It is particularly interesting to note that, when the initial entry angle is 85°, the tube is able to reach the 90° entry angle even at the higher receptor density of $\phi = 0.33$ (Supp. Fig. 9b). In the extreme case of $\phi = 1$ (Supp. Fig. 9c), the entry angle MWCNT tends to decrease, similar to the case when the initial entry angle $\theta_0$=45°. Supp. Fig. 10 shows similar simulations at $\theta_0$=15°, demonstrating nearly vertical tip entry at a very low initial entry angle. Supp. Fig. 11 summarizes the time evolution of entry angle for various selections of initial entry angle, cap geometry, binding strength and receptor density, all of which confirm the tip-entry mechanism.

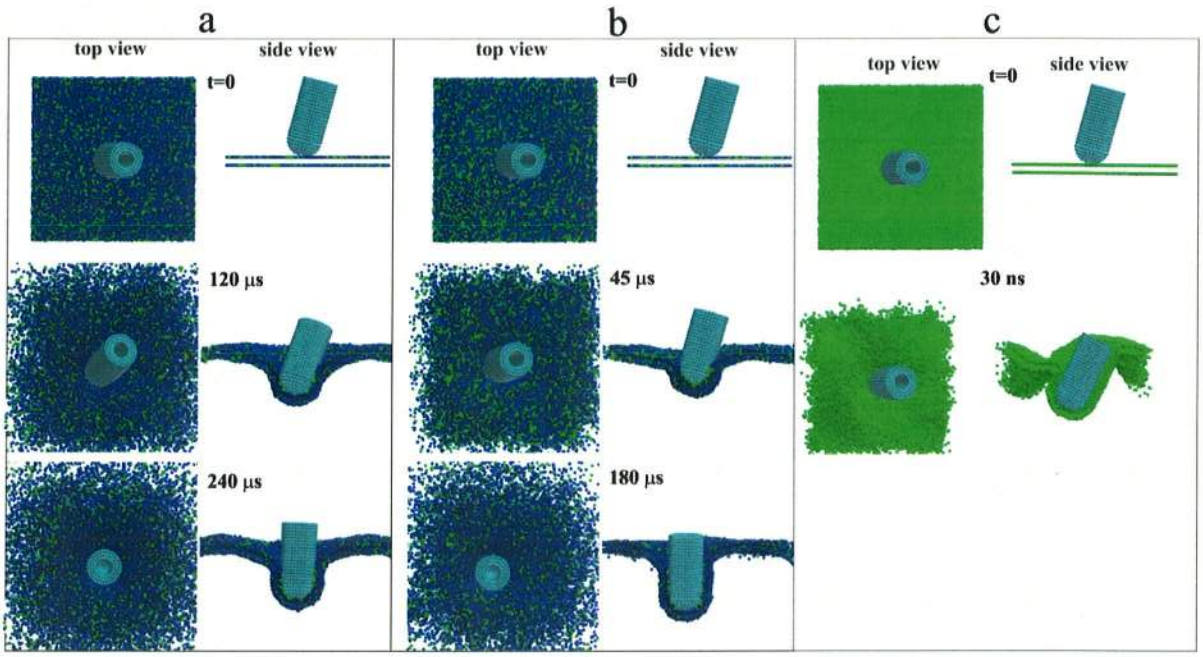


**Supplementary Figure 9. Time sequence of CGMD simulation results showing a MWCNT penetrating the cell membrane at an initial entry angle of θ0=85°. a,b,** With receptor (green) density $\phi = 0.25$ and $\phi = 0.33$, the MWCNTs is wrapped by the membrane and finally rotates to 90° before it is being fully wrapped. **c,** With the receptor density $\phi = 1$,the tube is wrapped at a low entry angle.

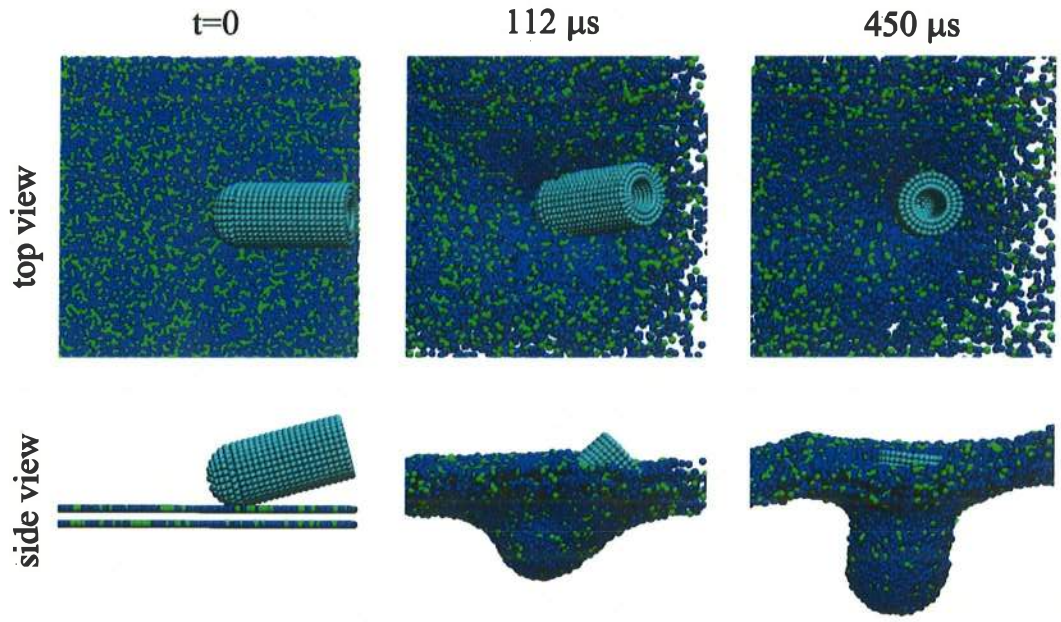


**Supplementary Figure 10. Time sequence of CGMD simulation results showing nanotubes penetrating the cell membrane at an initial entry angle of $\theta = 15^{\circ}$.** The fraction of receptor is $\phi = 0.25$.

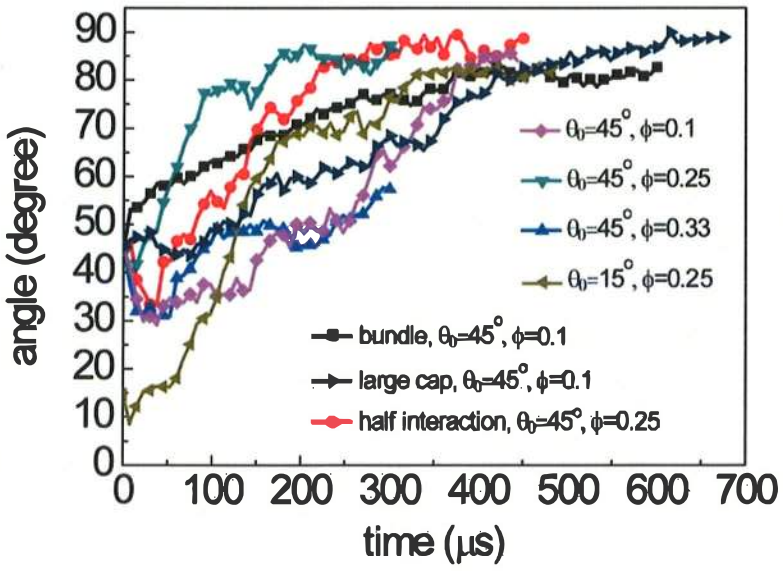


**Supplementary Figure 11. Evolution of the entry angle of various nanotubes with different caps, initial entry angles, receptor fractions and receptor interaction strengths.** The red profile indicates that the interaction strength between the particles of tube and receptor reduces to half, i.e. $0.5\varepsilon$.

## Supplementary References


[S1] Van Effenterre, D. & Roux, D. Adhesion of colloids on a cell surface in competition for mobile receptors. *Europhys. Lett.* **64,** 543–549 (2003).

[S2] Bell, G. I. Models for the specific adhesion of cells to cells. *Science* **200,** 618–627(1978).

[S3] Tzlil, S., Deserno, M., Gelbart, W. M. & Ben-Shaul, A. A statistical-thermodynamic model of viral budding. *Biophys. J.* **86,** 2037–2048 (2004).

[S4] Briggs, J. A. G., Wilk, T. & Fuller, S. D. Do lipid rafts mediate virus assembly and pseudotyping? *J. Gen. Virol.* **84**, 757–768 (2003).

[S5] Yang, K. & Ma Y. Q. Computer simulation of the translocation of nanoparticles with different shapes across a lipid bilayer. *Nature Nanotech.* **5,** 579-583 (2010).

[S6] Shi, X. H., Kong, Y. & Gao, H. J. Coarse grained molecular dynamics and theoretical studies of carbon nanotubes entering cell membrane. *Acta Mech.Sinica,* **24,** 161-169 (2008).